ACS APPLIED ENERGY MATERIALS

www.acsaem.org

Article

Investigation of Interactions between Carbazole-Based Quaternary Ammonium Salts and Lead-Based Perovskites

Matas Steponaitis,* Vidas Pakštas, Tomas Murauskas, Arnas Naujokaitis, Tadas Malinauskas, Vytautas Getautis, Vidmantas Gulbinas, and Marius Franckevičius*

Cite This: *ACS Appl. Energy Mater.* 2026, 9, 2701−2708

Read Online

ACCESS | Metrics & More | Article Recommendations | Supporting Information

ABSTRACT: Over a relatively short period of time, the power conversion efficiency of perovskite solar cells (PSCs) has increased from 3.8 to 27%. Despite this rapid progress, stability issues still remain a major challenge for widespread commercial application, thus motivating extensive research on perovskite surface defect passivation that would improve the longevity of PSCs. Although many reported passivation strategies are demonstrated under specific deposition conditions and device architectures, the reasons behind their effectiveness are not fully understood. In this study, we systematically examine quaternary ammonium and thiouronium organic salts as surface-passivating agents for triple-cation PSCs and compare their behavior with that of the commercially available sulfonium-based salt DMPESI. By combining photoluminescence (PL), time-resolved photoluminescence (trPL), X-ray photoelectron spectroscopy (XPS), liquid-state nuclear magnetic resonance (NMR), and device measurements, we show that different characterization techniques probe different features of organic−perovskite interactions. Although some treatments improve radiative recombination, as indicated by PL and trPL data, these results do not directly relate to the photovoltaic performance. Only the iodide-containing ammonium salt CzEAI shows device improvement consistent with XPS analysis. This work reveals the complex nature of defect passivation in PSCs.

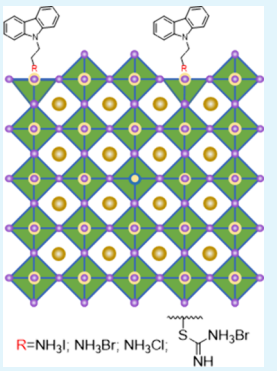

KEYWORDS: *perovskite, interaction, surface defects, organic salts, solar cells*

1. INTRODUCTION

Nowadays, record-breaking perovskite solar cells (PSCs) typically use perovskite surface passivation layers, which seem to lack reliable references despite being presented as crucial for achieving high efficiency and long-term stability.[1−3] The concept of surface defect passivation in PSCs came from silicon solar cells (SSCs), where a thin layer of material—often aluminum oxide (Al_2O_3) and silicon nitride (SiN_x)—was used to reduce the surface recombination of p-doped and n-doped silicon, respectively. However, since PSCs and SSCs differ in stability, energy levels, carrier mobility, etc., the same materials cannot be applied for passivation.[4] The closest material to becoming a standard for surface defect passivation in PSCs is phenethylammonium iodide (PEAI),[5] with some studies using it as a reference for their proposed new passivating molecules.[6−8] Record-breaking PSCs use a variety of molecules and strategies to passivate surface defects.[9] However, recently published works on surface passivation do not use a reference passivation layer for comparison.[10−12] Furthermore, the materials used for passivation have different deposition conditions, e.g., annealing temperature,[3,7,13,14] time of annealing,[3,14,15] perovskite composition,[3,7,15] concentration,[3,7,13] and perovskite preconditioning.[7,8,14] It is not always clear why certain conditions were used or what effect they had on the end result. Nevertheless, surface defect passivation is generally attributed to the interaction between the passivating molecule and uncoordinated lead ions.[7,13−15]

Organic surface-passivating molecules have been extensively studied to improve the quality of perovskite films and the performance of devices. Many studies have reported that the effectiveness of passivation can be assessed using optical techniques, such as photoluminescence (PL) and time-resolved photoluminescence (trPL), solution-phase measurements, such as nuclear magnetic resonance (NMR), or surface chemistry analytical techniques such as X-ray photoelectron spectroscopy (XPS). However, it is unclear to what extent these methods reflect the role of passivators during film formation and device operation. In this study, we synthesized and examined carbazole-based thiouronium and quaternary ammonium salts with different halogen counterions (Figure 1) to identify the most effective carbazole-based triple-cation perovskite surface passivator. Additionally, we tested the commercially available sulfonium-based salt DMPESI, given its recent success as a surface-passivating material in

Received: December 5, 2025
Revised: January 16, 2026
Accepted: February 5, 2026
Published: February 14, 2026

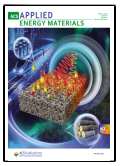

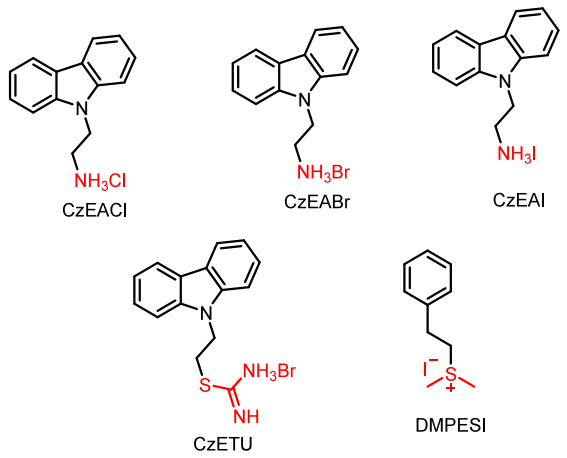

Figure 1. Structures of investigated molecules for perovskite surface passivation.

formamidinium lead iodide (FAPI)-based perovskite solar cells (PSCs).[3] While PL and trPL measurements indicated the most promising candidates, applying them in PSCs did not clearly correlate with the photocurrent efficiency (PCE). Further analysis using XPS and NMR also revealed a poor correlation between the optical response and the observed chemical interactions. Our results show that commonly used screening methods may not provide reliable results when evaluating passivating molecules. This highlights the need to combine optical, interfacial, and device data to better understand the interactions between passivating molecules and perovskite films.

2. RESULTS AND DISCUSSION

To investigate the passivation effect of organic quaternary ammonium, thiouronium, and sulfonium salts on the perovskite surface, PL and trPL measurements were employed to probe near-surface defect states and their influence on charge-carrier recombination dynamics. This approach is based on the concept that defects, such as unreacted Pb^{2+}, promote nonradiative recombination and can reduce the PL intensity and carrier lifetime. Therefore, changes in PL intensity and/or carrier lifetime are commonly used as indicators of defect passivation when investigating the interactions between organic salts and lead-based perovskites.[1,2,13,16] However, perovskites used in optoelectronics applications are known to exhibit significant batch-to-batch[17−20] and even sample-to-sample variations.[21] To minimize sample-to-sample variability, PL and trPL measurements were performed on films prepared from the same perovskite samples. For the concentration-dependent studies, perovskite-coated glass substrates were

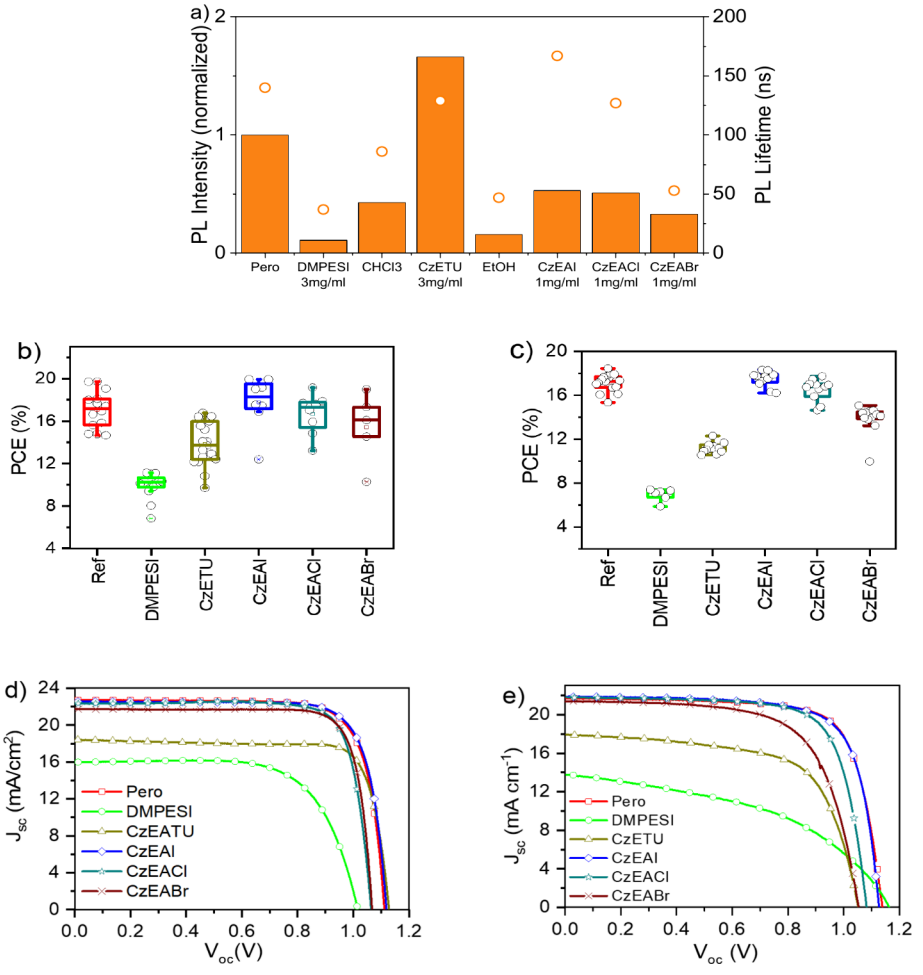

Figure 2. (a) Normalized PL intensity (represented by bars) and average PL lifetimes obtained from trPL (symbols) before and after treatment with the optimal concentration of investigated compounds and with pure solvents; (b) PCEs of p-i-n devices; (c) PCEs of n-i-p devices; (d) *J*−*V* curves of champion p-i-n devices; and (e) *J*−*V* curves of champion n-i-p devices.

https://doi.org/10.1021/acsaem.5c03857
ACS Appl. Energy Mater. 2026, 9, 2701−2708

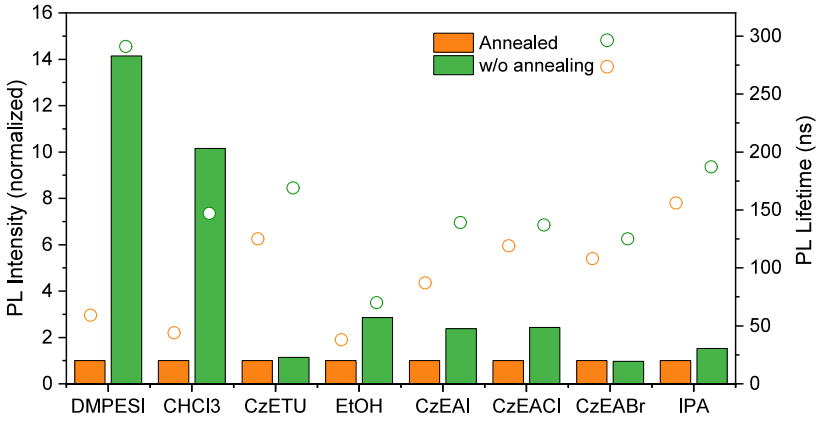

Figure 3. Normalized PL intensity (represented by bars) and average PL lifetimes obtained from trPL (symbols) of treated perovskite samples annealed and without annealing.

divided into multiple pieces, which were subsequently treated with different concentrations of the investigated passivating molecules, meanwhile one piece from each substrate was kept as an untreated reference sample (Figure S1).

The highest PL intensities and trPL lifetimes for the films treated with DMPESI (deposited from chloroform) and CzETU (deposited from ethanol) were obtained at concentrations of 3 mg/mL, while for CzEAI (deposited from isopropanol), the strongest PL intensity was at 1 mg/mL. Due to the limited solubility in IPA, the quaternary ammonium salts CzEACl and CzEABr were applied at a concentration of 1 mg/mL. Figure 2a summarizes the integrated PL intensities and average trPL lifetimes of pristine perovskite films and films treated with passivating materials at their optimal concentrations, as well as with pure solvents. Among the investigated compounds, the thiouronium salt CzETU shows a clear improvement in PL intensity and carrier lifetime compared to the pristine perovskite film; however, this effect is concentration dependent, with the most pronounced response observed at 3 mg/mL. In contrast, the perovskite treatment with the quaternary ammonium salts CzEACl and CzEABr, as well as with the sulfonium salt DMPESI, results in reduced PL intensity and carrier lifetime, compared to the untreated films.

To verify that the observed changes in PL and trPL originate from the passivating materials rather than from the solvents used for their deposition, the PL and trPL of perovskite films were also performed on perovskite films treated with pure $CHCl_3$, IPA, and EtOH (see Figures 2a and S2). As shown in Figures 2a and S2, treatment of the perovskite surface with each of these solvents results in a reduction in both PL intensity and charge-carrier lifetime. This behavior is indicative of increased nonradiative recombination at the perovskite surface. These observations suggest that even solvent treatment alone can modify the surface defect states of perovskite films, independent of the passivating molecules used, which is consistent with previous reports.[22]

The solvent-induced changes observed in PL and trPL motivated further investigation of the effect of post-treatment annealing. This investigation was prompted by previous literature reports indicating that, contrary to common practice, surface-passivated perovskite films are rather often characterized without an additional annealing step.[2,7,8] The investigated materials were applied at concentrations corresponding to the best PL and trPL responses identified previously: 3 mg/mL for DMPESI and CzETU, and 1 mg/mL for CzEAI, CzEABr, and CzEACl. It is also worth noting that DMPESI was deposited from chloroform and CzETU from EtOH, while the remaining materials were from IPA. Figures 3 and S3 show that with few exceptions, nonannealed films exhibit higher PL intensities and longer charge-carrier lifetimes than annealed films.

The most pronounced annealing-induced changes in PL and trPL were observed for films treated with DMPESI and pure $CHCl_3$. Noticeable effects were also observed for carbazole-based derivatives (CzEAI, CzEACl) and alcohol (EtOH, IPA)-treated films. These changes are most likely related to solvent–perovskite interactions during the post-treatment process, which can modify surface defect states or induce surface rearrangements.[23,24] Though PL and trPL mainly provide information about radiative recombination processes of defect states located at the surface, the changes in PL intensity or carrier lifetime do not necessarily correlate with photovoltaic performance, which is strongly influenced by interfaces with charge-selective layers, as discussed below.

To determine whether the changes observed in PL and trPL correlate with device operation, p-i-n PSCs with the architecture ITO/MeO2 Pacz/perovskite (with or without a passivator)/PCBM/BCP/Ag were fabricated. Devices labeled EtOH, IPA, and $CHCl_3$ were prepared by treating the perovskite layer with the corresponding pure solvents under the same conditions as those used for solutions containing passivating molecules, allowing to independently access the solvent effect on the device performance. Comparison of pure solvent-treated PCSs with the reference devices reveals that the most notable change is observed for perovskite samples treated with EtOH (Figure S4). This resulted in a reduced average V_{oc} and a large spread in *FF* and J_{sc} values. This behavior is consistent with previous literature reports attributing ethanol treatment to partial loss of organic cations from the perovskite surface.[22]

The influence of the investigated passivating compounds on the photovoltaic performance of p-i-n devices varies significantly (Figure S5 and 2b). Devices treated with DMPESI exhibit reduced photovoltaic parameters, particularly J_{sc}, which may be associated with an interfacial energy-level mismatch between the modified perovskite surface and PCBM layer. While treatment with CzETU results in a slight increase in V_{oc} and a reduced V_{oc} spread, it negatively affects the short-circuit current by decreasing it, similarly to DMPESI. Among the investigated carbazole-based salts, only CzEAI yields a slight

https://doi.org/10.1021/acsaem.5c03857
ACS Appl. Energy Mater. 2026, 9, 2701−2708

improvement in device performance, associated with a minor increase in the average V_{oc}. In contrast, CzEACl and CzEABr negatively impact device performance, mainly due to reductions in V_{oc} and J_{sc}, respectively.

As many surface passivation studies reported in the literature are conducted using n-i-p device architectures, the passivating effect of DMPESI and the investigated carbazole-based thiouronium and quaternary ammonium salts were further evaluated in n-i-p perovskite solar cells with the architecture ITO/SnO_2/perovskite/passivator (with or without passivator)/Spiro-OMeTAD/Ag (Figure S6 and 2c). In this configuration, perovskite treatment with DMPESI results in an increased V_{oc}, which is consistent with defect passivation at the perovskite surface. However, this improvement is accompanied by evident reduction of other photovoltaic parameters, suggesting hindered charge-carrier extraction at the perovskite/hole transport layer interface, expectedly due to the modulation in energy levels of the treated perovskite surface. Meanwhile, CzETU has a significant negative impact on device performance, leading to a decrease in all photovoltaic parameters. This behavior is inconsistent with increased PL intensity and trPL lifetime values observed for CzETU-treated perovskite films, as well as with the increased V_{oc} measured in p-i-n devices. As discussed above, surface passivation does not necessarily correlate between improved photovoltaic performance and optical properties, and the effect of surface treatments is expectedly dependent on device architecture and energy-level alignment at the interface.[25]

To further evaluate whether the reduced performance in n-i-p devices originates from the excess of passivator on the perovskite surface, additional devices were fabricated using a lower CzETU concentration of 1 mg/mL (Figure S7). Although lowering the concentration improved the performance of the devices compared to PSCs treated with 3 mg/mL of CzETU, no improvement related to the reference device was observed. Furthermore, the photovoltaic parameters of PSCs treated with 1 mg/mL of CzETU resemble those of the reference devices, suggesting that the material has little effect on device performance at low concentrations. In the case of PSCs treated with other carbazole-based ionic salts, CzEAI-treated devices exhibit a modest improvement in photovoltaic performance, characterized by a reduced V_{oc} spread. In contrast, treatment of perovskite devices with CzEACl and CzEABr led to decreases in V_{oc} and *FF*, respectively.

To exclude morphology-related effects, scanning electron microscopy (SEM) was performed on pristine and passivated perovskite films. As shown in Figure S8, no significant changes in grain size or surface coverage were observed after treatment with carbazole-based salts, indicating that the differences in optoelectronic properties and device performance are unlikely to originate from morphological variations in these compounds. On the other hand, perovskite surface-treated with DMPESI forms larger grains that should improve the performance of PSCs;[26] although, the opposite is observed. Furthermore, a notable visual change occurs after treating the perovskite sample with a DMPESI solution (Figure S9). However, the color change disappears after annealing the sample. We hypothesize that DMPESI causes recrystallization of the entire perovskite layer, causing energy levels to change hindering effective charge transport and in turn reducing the photovoltaic performance of PSCs.

To further investigate whether the treatment-induced luminescence and device performance variations are associated with structural modifications of the perovskite films, XRD was performed on pristine and passivated perovskite films. XRD measurements performed on films treated with the investigated materials at various concentrations are shown in Figure S10. While Figure 4 presents XRD diffractograms of perovskite

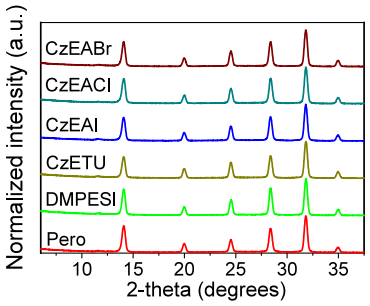

Figure 4. Normalized grazing angle XRD of perovskite samples treated with optimal concentrations of each investigated material (CzEAI, CzEACl, and CzEABr were deposited from IPA, while CzETU and DMPESI were deposited from EtOH and chloroform, respectively).

films treated with the investigated materials at their optimal concentrations. The XRD patterns revealed no significant differences between the samples, suggesting that the crystalline structure of the perovskite remains unchanged. Additionally, grazing angle XRD measurements were performed on samples treated only with pure solvents (Figure S11). While films treated with $CHCl_3$ showed no significant changes, samples treated with IPA and EtOH exhibited additional peaks at 12.66°, attributed to unreacted PbI_2.[22] These findings could explain the difference in performance between PSCs treated with pure solvents; however, they do not explain the discrepancies among PL, trPL, and device performance when passivating materials are used.

Lastly, we used XRD to determine whether annealing the passivated samples altered the crystalline structure of the perovskites (Figure S12). As with previous XRD measurements, practically no annealing-induced changes were observed. It is likely that the interactions between the solvent and the perovskite that cause the difference in the PL and trPL between the samples before and after annealing are disrupted when the sample is annealed. Therefore, annealing does not affect the performance of the devices, as the deposition of other layers removes the attached solvent molecules during spin coating or inside the vacuum chamber under reduced pressure. However, it is important to note that if perovskite thin films are not annealed after the deposition of passivating materials, this could distort the PL and trPL data, which could misdirect further investigation.

To gain more insight into the chemical interactions occurring at the perovskite/passivating molecule interface, XPS was used to measure the difference in binding energies (BE) of elements between the pristine perovskite film and films treated with the sulfonium salt DMPESI and carbazole-based salts containing either thiouronium or quaternary ammonium groups with different counterions. The most pronounced changes were observed in the Pb $4f_{7/2}$ region (Figure 5), while analysis of N 1s core level proves that carbazole derivatives remain on the surface of perovskite during measurements at ultrahigh vacuum (Figure S13).

https://doi.org/10.1021/acsaem.5c03857
ACS Appl. Energy Mater. 2026, 9, 2701−2708

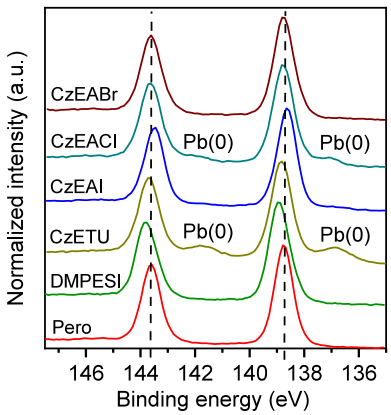

Figure 5. XPS data of the Pb $4f_{7/2}$ core level of pristine and treated perovskite thin films.

The changes in BE indicate alterations in the local chemical environment of the atom—a shift toward higher BE indicates reduced electron density (deshielding), whereas the shift toward lower BE indicates increased electron density and enhanced shielding of the atom. From this perspective, the partial passivation of undercoordinated Pb^{2+} site is expected to manifest itself as a downshift of the Pb $4f_{7/2}$ peak position.[27] As shown in Figure 5, treatment with CzEAI results in a downshift of the Pb $4f_{7/2}$ core level, indicating an increased electron density around Pb atoms, which suggests possible chemical interaction with Pb-related surface defects.

In contrast, perovskite treatment with DMPESI and CzETU causes deshielding of the Pb $4f_{7/2}$ core level, which is accompanied by reduced device performance, whereas CzEACl and CzEABr had no effect on the peak position. Furthermore, deposition of the thiouronium salt CzETU and quaternary ammonium salt with chlorine counterion CzEACl, resulted in the formation of Pb(0) species, which are commonly associated with reduced long-term stability of perovskites films.[28]

To further investigate these interactions, liquid-state NMR was employed. NMR spectra were recorded for each passivating molecule, both without any additives and in the presence of PbI_2, to observe if any chemical shifts are noticeable in the presence of PbI_2, which in turn would demonstrate the interaction between PbI_2 and the investigated material. Prior to conducting the measurements, however, it was necessary to determine whether the concentration of PbI_2 affects the chemical shifts between the samples. To this end, CzETU solutions in DMSO were prepared with PbI_2 concentrations of 0.1, 0.5, and 1 M. The measurements revealed only negligible differences in chemical shifts across the different concentrations (see Supporting Information (SI) NMR shifts); therefore, a 0.1 M lead iodide was used for further study. We note that the shifts observed in our ^{13}C NMR data are rather small; however, they are similar in magnitude to those reported in the work of Chen et al. and therefore are unlikely to originate from experimental noise.[12]

Initial measurements in DMSO showed that CzETU and CzEACl exhibit significant hydrogen chemical shifts in the ^{1}H NMR spectra of singlets representing the NH^{3+} functional groups. This indicates an interaction with PbI_2 through ionic ammonium groups. Furthermore, CzETU and CzEACl demonstrated notable shifts in the carbon signals of the ^{13}C NMR spectra corresponding to carbons directly bonded to the ionic group (Figure 6). Since DMSO is known to interact with lead salts,[29] additional NMR measurements were performed in

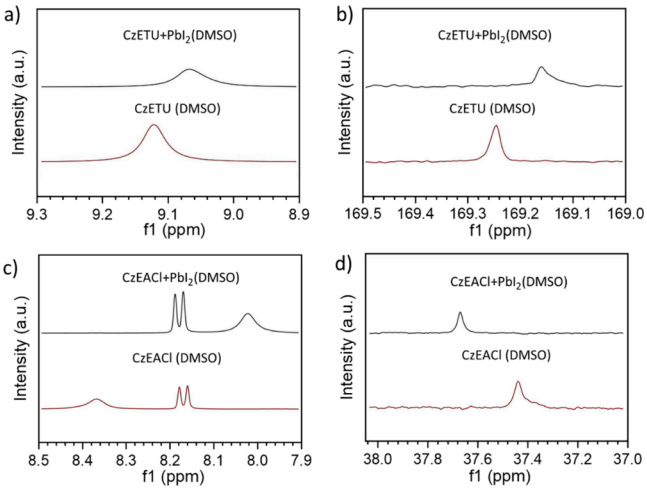

Figure 6. NMR spectra shifts of CzETU (top) and CzEACl (bottom) in DMSO-d_6.

DMF to determine if the interaction was solvent-specific (see Figures S14 and S15). Chemical shifts due to interaction were still noticeable for CzETU and CzEACl in DMF, although they were of a magnitude smaller than that in DMSO. Interestingly, the CzEABr molecule, which showed a negligible chemical shift in the ^{1}H spectrum in DMSO, exhibited clear ^{1}H and ^{13}C chemical shifts in DMF. This demonstrates that solvents can influence the interaction between PbI_2 and the investigated compound.

Surprisingly, our NMR measurements showed no interaction between the quaternary ammonium salt, CzEAI, or the sulfonium salt, DMPESI, and lead iodide (Figures S14 and S15), despite previous reports of their excellent performance in FAPI- and CsFAPI-based solar cells, respectively.[3,8] Additional NMR measurements were conducted to investigate this discrepancy more deeply. These measurements were conducted between DMPESI and each individual precursor used to prepare the perovskite solution; however, no chemical shifts were observed. These findings suggest two possible explanations. First, different perovskites require distinct passivating molecules to effectively passivate their defects due to their different surface chemistry. Second, while observable NMR chemical shifts in solution demonstrate a material's potential to bind to lead defects, they might not accurately represent the interaction happening at the liquid−solid interface during spin coating and annealing. Overall, these results suggest that solution-based investigations may not fully capture the complexity of the perovskite−molecule interactions during film formation.

3. CONCLUSIONS

Our results demonstrate that different characterization techniques probe distinct aspects of perovskite surface interactions with organic molecules. In particular, improved radiative recombination, as observed from PL and trPL measurements, does not necessarily correlate with enhanced photovoltaic performance, which is strongly influenced by the interfacial energy-level alignment as well as by device-architecture-dependent charge-carrier extraction. The com-

https://doi.org/10.1021/acsaem.5c03857
ACS Appl. Energy Mater. 2026, 9, 2701−2708

monly used methods such as PL, trPL, NMR, XRD, and XPS therefore provide complementary but not identical information about passivation processes. Optical measurements are primarily sensitive to surface recombination but do not directly reveal the chemical nature of the molecular interactions between perovskite and passivating molecules. In contrast, liquid-state NMR could reflect potential interactions between lead ions and other molecules in solution but cannot accurately predict interactions between passivators and the perovskite surface due to spatial constraints for bonding in the solid state. Structural techniques such as XRD lack the sensitivity to detect surface changes in perovskite because they probe the bulk of the perovskite layer. In contrast, XPS offers direct insight into chemical changes at the surface, providing more direct information related to defect passivation.

Device measurements demonstrated the importance of negatively charged halogen ions in carbazole-based salts. Among the investigated materials, only devices treated with ammonium salt CzEAI containing iodine, as the counterion showed improvement in photovoltaic characteristics, which correlated with the XPS data. Moreover, noticeable differences in performance were observed between p-i-n and n-i-p PSC devices treated with DMPESI and CzETU, highlighting that the effectiveness of perovskite surface passivation is also strongly architecture dependent.

Overall, our results reveal that the apparent discrepancies between different characterization techniques do not reflect inconsistencies but rather suggest the complex nature of defect passivation and charge-carrier extraction in PSCs. Instead of identifying a single universal passivating molecule, this work demonstrates the need to understand why the improvements observed in one or another characterization method do not necessarily translate into an improvement of the device performance on different architectures.

4. EXPERIMENTAL SECTION

4.1. Materials

ITO-patterned substrates 20 × 15 mm were purchased from Ossila. MeO-2PACz, lead(II) Bromide (>98.0%), and lead(II) iodide (>98.0%) were purchased from TCI. Formamidinium iodide (FAI) (>99.99%) and methylammonium bromide (>99.99%) were purchased from Greatcell Solar Materials. Cesium iodide (CsI) (>99.999%), PCBM (99.5%), BCP (>99.99%), *N*,*N*-dimethylformamide (DMF, anhydrous 99.8%), dimethyl sulfoxide (anhydrous DMSO, >99.9%), and chlorobenzene (CB, 99.8%) were purchased from Sigma-Aldrich. Tin(IV) oxide (SnO_2, 15% in H_2O colloidal dispersion) was purchased from Alfa Aesar. Silver pellets (99.99%) for evaporation were purchased from Kurt J. Lesker, fast-drying conductive silver ACHESON 1415 was purchased from PLANO GmbH, and DMPESI was purchased from Dyenamo. Chemicals for the synthesis were purchased from Sigma-Aldrich and TCI Europe and used as received without further purification. Solvents used for deposition of the investigated materials and BCP were purchased from Eurochemicals and further purified by removing oxygen and water by previously known procedures using molecular sieves, sodium, and benzophenone. The course of the reactions was monitored by TLC (thin layer chromatography) on ALUGRAM SIL G/UV254 plates and developed with UV light. Silica gel (grade 9385, 230−400 mesh, 60 Å, Aldrich) was used for column chromatography. ^{1}H and ^{13}C NMR spectra were taken on a Bruker Avance III 400 (400 MHz) spectrometer at room temperature. Chemical shifts, expressed in δ (ppm), are relative to a $(CH_3)_4Si$ (TMS, 0 ppm) internal standard. Elemental analysis was performed with an Exeter Analytical CE-440 elemental analyzer, Model 440 C/H/N/.

4.2. PL and trPL Measurements

Fluorescence spectra and decay kinetics were measured using an Edinburgh Instruments F900 time-correlated single-photon counting fluorescence spectrometer. The picosecond pulsed diode laser EPL-470, emitting 72 ps pulses at 470 nm with a repetition rate of 50 MHz (100 ns), was used for sample excitation. The time resolution of the setup was several hundred picoseconds after application of apparatus function deconvolution.

4.3. XRD Measurements

XRD patterns of the perovskite thin films were measured using an X-ray diffractometer SmartLab (Rigaku) equipped with a 9 kW rotating Cu anode X-ray tube. Grazing-incidence XRD (GIXRD) method was used in a 2θ range of 5−75° with a step size of 0.02° (in 2θ scale) and counting time of 1 s per step. An angle between the parallel beam of X-rays and a specimen surface (ω angle) was adjusted to 0.5° degrees. Phase identification was performed using the PDXL software package (Rigaku) and ICDD powder diffraction database PDF-4+ (2024 release).

4.4. XPS Measurements

X-ray photoelectron spectroscopy (XPS) measurements were performed by using a Kratos Axis Supra instrument equipped with a monochromatic Al Kα radiation source (15 kV, 25 mA). XPS enables the identification of all elements except hydrogen and helium and provides surface-sensitive analysis with a probing depth of approximately 5−7 nm. Calibration of the spectrometer's work function was done using the Au $4f_{7/2}$ peak of metallic gold, set at a binding energy (BE) of 83.96 eV. Additionally, the energy scale was adjusted to align the Cu $2p_{3/2}$ peak of metallic copper to 932.62 eV. To compensate for surface charging, all measurements utilized the Kratos charge neutralization system. The survey spectra were collected over a 300 × 700 μm^2 analysis area at a pass energy of 160 eV, while high-resolution spectra were acquired by using the same area but at a reduced pass energy of 20 eV. All BEs were corrected by referencing the main C 1s peak of adventitious carbon to 284.8 eV. Data analysis was conducted using the CasaXPS software package (version 2.3.26PR1.0).

4.5. Device Fabrication

4.5.1. Substrate Preparation. The ITO substrates were cleaned sequentially for 10 min with a 0.5% Hellmanex solution in distilled water, acetone, and isopropyl alcohol in an ultrasonic bath. After that, directly before HTM or ETM deposition, the substrates were treated in a UV−ozone cleaner for 15 min. All except SnO_2 layers were deposited in a nitrogen-filled glovebox (MBRAUN).

4.5.2. Perovskite Solution Preparation. CsI (0.08 M), FAI (1.10 M), PbI_2 (1.15 M), MABr (0.2 M), and $PbBr_2$ (0.2 M) were dissolved in anhydrous DMF/DMSO (4:1 in volume). The precursor solution was heated at 70 °C for 1.5 h and then filtered with a 0.45 μm poly(tetrafluoroethylene) (PTFE) filter prior to use.

4.5.3. SAM Layer Preparation for p-i-n Solar Cells. 0.5 mg of MeO-2PACz (0.5 mg) was added to 1 mL of anhydrous 2-propanol and then sonicated for 10 min in an ultrasonic bath. Before spin-coating, the solution was filtered through a 0.45 μm PTFE, and a few drops of anhydrous DMF were added. 100 μL of the solution was spin-coated at 3000 rpm for 30 s onto cleaned ITO substrates and subsequently annealed at 100 °C for 10 min.

4.5.4. SnO_2 Layer Preparation for n-i-p Solar Cells. SnO_2, 15% in H_2O colloidal dispersion, was diluted with distilled water in a ratio of 1:4 and then sonicated for 30 min in an ultrasonic bath. Afterward, 100 μL of the solution was spin-coated at 3000 rpm for 30 s onto cleaned ITO substrates that had Kapton tape at the short edges in order to secure conductive contacts for further device measurements. Then, the samples were annealed on a hot plate for 30 min at 150 °C. Subsequently, the samples were ozonated for 30 min in a UV−ozone cleaner.

4.5.5. Preparation of Solutions of Investigated Material. DMPESI was dissolved in anhydrous chloroform at various concentrations. For concentrations above 1 mg/mL, the vial needed

https://doi.org/10.1021/acsaem.5c03857
ACS Appl. Energy Mater. 2026, 9, 2701−2708

to be heated at 70−100 °C for a few min in order to fully dissolve the investigated compound.

CzETU and CzEAI were dissolved at various concentrations in EtOH and IPA, respectively.

Due to the relatively poor solubility, 1 mg of CzEACl or CzEABr was added to 1 mL of IPA and sonicated for 10 min at 30 °C. Afterward, the remaining material that did not dissolve was filtered off through a 0.45 μm PTFE filter.

For every experiment or new batch, the solutions were made fresh. Reference devices did not contain this layer.

4.5.6. p-i-n Solar Cells. Perovskite film was formed by spin-coating 100 μL of perovskite precursor solution onto the SAM-coated ITO surface using a two-step deposition program: the first step at 1000 rpm for 10 s, followed by the second step at 6000 rpm for 30 s. Ten seconds before the end of the second step, 180 μL of CB was dropped onto the spinning substrate. Subsequently, the perovskite layer was annealed at 100 °C for 30 min. In an attempt to passivate the surface of perovskite films, 120 μL of either investigated material was spin-coated dynamically on top of the perovskite layer at a speed of 4000 rpm for 20 s and annealed for 10 min at 100 °C. A layer of PCBM was formed on top of perovskite from a 20 mg/mL solution in anhydrous CB at a speed of 3000 rpm for 30 s, followed by annealing at 100 °C for 5 min. Afterward, a 0.5 mg/mL solution of BCP in anhydrous EtOH was deposited at 4,000 rpm for 35 s (ramp 500 rpm), followed by annealing at 100 °C for 5 min. Finally, a 100 nm thick Ag electrode was thermally deposited under vacuum to complete the devices.

4.5.7. n-i-p Solar Cells. Perovskite film was formed by spin-coating 100 μL of perovskite precursor solution onto the SnO_2-coated ITO surface using a two-step deposition program: the first step at 1,000 rpm for 10 s, followed by the second step for 6000 rpm for 30 s. Ten seconds before the end of the second step, 180 μL of CB was dropped onto the spinning substrate. Subsequently, the perovskite layer was annealed at 100 °C for 30 min. In an attempt to passivate the surface of perovskite films, 120 μL of either investigated material was spin-coated dynamically on top of the perovskite layer at a speed of 4000 rpm for 20 s and annealed for 10 min at 100 °C. Spiro-OMeTAD layer was deposited on top of the perovskite layer by dynamically spin-coating at 4000 rpm for 20 s from a solution of 100 mg Spiro-OMeTAD in 1 mL of CB. This solution was doped with 20 μL of LiTFSI stock solution (516 mg/mL in anhydrous acetonitrile), 8 μL of FK-209 stock solution (376 mg/mL in anhydrous acetonitrile), and 36 μL of 4-tBP prior to spin-coating. Afterward, the samples are moved from the glovebox to the desiccator and kept overnight. The following day, 100 nm of Ag is evaporated on top, and the devices are moved back to the desiccator for 4 more hours before being measured.

4.6. Solar Cell Characterization

The photovoltaic devices were characterized in ambient conditions with the room temperature around 20−24 °C and ∼35% relative humidity under AM1.5G simulated sunlight using a Sinus-70 Solar simulator. The measurement parameters for p-i-n devices were as follows: intensity of 100 mW/cm^2, flash time of 10,000 ms, trigger delay of 30 ms, 1000 measurement steps, a minimum voltage of −0.05 V, and a maximum voltage of 1.2 V. n-i-p device measurement differed from p-i-n by the number of measurement steps, which was 300 instead of 1000, and by the addition of a 28 ms delay between voltage sweep steps. On each substrate, there were 8 devices with an area of 0.0256 cm^2. The areas were defined by using Ossila stainless-steel shadow masks placed in direct contact with the glass side of the substrates within enclosed sample holders.

■ ASSOCIATED CONTENT

Supporting Information

The Supporting Information is available free of charge at https://pubs.acs.org/doi/10.1021/acsaem.5c03857.

Synthesis, normalized PL and trPL of perovskite films treated with the investigated materials of various concentrations, normalized PL and trPL of perovskite films treated with different solvents, normalized PL and trPL of annealed vs not annealed perovskite samples with various treatments, box plots of photovoltaic characteristics of p-i-n PSCs treated with different solvents, box plots of photovoltaic characteristics of p-i-n architecture PSCs treated with the investigated materials, box plots of photovoltaic characteristics of n-i-p architecture PSCs treated with the investigated materials, box plots of photovoltaic characteristics of n-i-p PSCs treated with different concentrations of CzETU, surface morphology of perovskite samples of pristine and treated samples, DMPESI-treated perovskite samples before annealing, grazing angle XRD of perovskite films treated with varying concentrations of investigated materials, normalized grazing angle XRD of perovskite films treated with different solvents, normalized grazing angle XRD of annealed vs not annealed perovskite samples, XPS data of N 1s core level of treated perovskite thin films, NMR spectra of investigated compounds in DMSO-d_6, NMR spectra of investigated compounds in DMF-d_7, and NMR shifts (PDF)

■ AUTHOR INFORMATION

Corresponding Authors

Matas Steponaitis − *Center for Physical Sciences and Technology (FTMC), Vilnius LT-10257, Lithuania;* orcid.org/0000-0002-4696-6121; Email: matas.steponaitis@ftmc.lt

Marius Franckevičius − *Center for Physical Sciences and Technology (FTMC), Vilnius LT-10257, Lithuania;* orcid.org/0000-0001-8020-7201; Email: marius.franckevicius@ftmc.lt

Authors

Vidas Pakštas − *Center for Physical Sciences and Technology (FTMC), Vilnius LT-10257, Lithuania*

Tomas Murauskas − *Institute of Chemistry, Faculty of Chemistry and Geosciences, Vilnius University, Vilnius LT-03225, Lithuania*

Arnas Naujokaitis − *Center for Physical Sciences and Technology (FTMC), Vilnius LT-10257, Lithuania;* orcid.org/0000-0002-4950-5718

Tadas Malinauskas − *Department of Organic Chemistry, Kaunas University of Technology, Kaunas LT-50254, Lithuania;* orcid.org/0000-0002-5478-6550

Vytautas Getautis − *Department of Organic Chemistry, Kaunas University of Technology, Kaunas LT-50254, Lithuania;* orcid.org/0000-0001-7695-4677

Vidmantas Gulbinas − *Center for Physical Sciences and Technology (FTMC), Vilnius LT-10257, Lithuania*

Complete contact information is available at: https://pubs.acs.org/10.1021/acsaem.5c03857

Funding

This research was funded by the Research Council of Lithuania (LMTLT), agreement no. P-PD-23-035.

Notes

The authors declare no competing financial interest.

REFERENCES

(1) Khadka, D. B.; Shirai, Y.; Yanagida, M.; Ota, H.; Lyalin, A.; Taketsugu, T.; Miyano, K. Defect passivation in methylammonium/bromine free inverted perovskite solar cells using charge-modulated molecular bonding. *Nat. Commun.* **2024**, *15*, 882.

(2) Wang, S.; Yao, C.; Li, L.; Huang, T.; Tan, S.; Shi, P.; Jin, S.; Zhu, C.; Yang, Y.; Zhu, B.; Xue, J.; Wang, R. Enhanced passivation durability in perovskite solar cells via concentration-independent passivators. *Joule* **2024**, *8* (4), 1105−1119.

(3) Suo, J.; Yang, B.; Mosconi, E.; Bogachuk, D.; Doherty, T. A. S.; Frohna, K.; Kubicki, D. J.; Fu, F.; Kim, Y.; Er-Raji, O.; Zhang, T.; Baldinelli, L.; Wagner, L.; Tiwari, A. N.; Gao, F.; Hinsch, A.; Stranks, S. D.; De Angelis, F.; Hagfeldt, A. Multifunctional sulfonium-based treatment for perovskite solar cells with less than 1% efficiency loss over 4,500-h operational stability tests. *Nat. Energy* **2024**, *9*, 172−183.

(4) Liu, J.; He, Y.; Ding, L.; Zhang, H.; Li, Q.; Jia, L.; Yu, J.; Lau, T. W.; Li, M.; Qin, Y.; Gu, X.; Zhang, F.; Li, Q.; Yang, Y.; Zhao, S.; Wu, X.; Liu, J.; Liu, T.; Gao, Y.; Wang, Y.; Dong, X.; Chen, H.; Li, P.; Zhou, T.; Yang, M.; Ru, X.; Peng, F.; Yin, S.; Qu, M.; Zhao, D.; Zhao, Z.; Li, M.; Guo, P.; Yan, H.; Xiao, C.; Xiao, P.; Yin, J.; Zhang, X.; Li, Z.; He, B.; Xu, X. Perovskite/silicon tandem solar cells with bilayer interface passivation. *Nature* **2024**, *635*, 596−603.

(5) Jiang, Q.; Zhao, Y.; Zhang, X.; Yang, X.; Chen, Y.; Chu, Z.; Ye, Q.; Li, X.; Yin, Z.; You, J. Surface passivation of perovskite film for efficient solar cells. *Nat. Photonics* **2019**, *13*, 460−466.

(6) Azam, M.; Du, T.; Wan, Z.; Zhao, H.; Zeng, H.; Wei, R.; Brabec, C. J.; Luo, J.; Jia, C. Dual Functionality of Charge Extraction and Interface Passivation by Self-Assembled Monolayers in Perovskite Solar Cells. *Energy Environ. Sci.* **2024**, *17* (19), 6974−7016.

(7) Tumen-Ulzii, G.; Auffray, M.; Klotz, D.; Harrington, G. F.; Chen, X. K.; Balijapalli, U.; Vediyappan, V.; Nakamura, N.; Feng, Z.; Takekuma, K.; Fujita, Y.; Wang, P.; Yamada, S.; Tamada, K.; Batmunkh, M.; Zhong, Y. L.; Mathevet, F.; Salway, H.; Anaya, M.; Stranks, S. D.; Matsushima, T.; Adachi, C. Defect Passivation by Pyridine-Carbazole Molecules for Efficient and Stable Perovskite Solar Cells. *ACS Appl. Energy Mater.* **2022**, *5* (12), 15819−15827.

(8) Shi, Z.; Guo, R.; Luo, R.; Wang, X.; Ma, J.; Feng, J.; Niu, X.; Alvianto, E.; Jia, Z.; Guo, X.; Liang, H.; Chen, J.; Li, Z.; Sun, K.; Jiang, X.; Wu, Y.; Müller-Buschbaum, P.; Hu, W.; Hou, Y. "T-shaped" Carbazole Alkylammonium Cation Passivation in Perovskite Solar Cells. *ACS Energy Lett.* **2024**, *9* (2), 419−427.

(9) Garai, R.; Gupta, R. K.; Iyer, P. K. Trap State Passivation for Stabilizing Perovskite Solar Cells via Multifunctional Molecules. *Acc. Mater. Res.* **2023**, *4* (7), 560−565.

(10) Chin, X. Y.; Turkay, D.; Steele, J. A.; Tabean, S.; Eswara, S.; Mensi, M.; Fiala, P.; Wolff, C. M.; Paracchino, A.; Artuk, K.; Jacobs, D.; Guesnay, Q.; Sahli, F.; Andreatta, G.; Boccard, M.; Jeangros, Q.; Ballif, C. Interface passivation for 31.25%-efficient perovskite/silicon tandem solar cells. *Science* **2023**, *381* (6653), 59−63.

(11) Xu, J.; Chen, H.; Grater, L.; Liu, C.; Yang, Y.; Teale, S.; Maxwell, A.; Mahesh, S.; Wan, H.; Chang, Y.; Chen, B.; Rehl, B.; Park, S. M.; Kanatzidis, M. G.; Sargent, E. H. Anion optimization for bifunctional surface passivation in perovskite solar cells. *Nat. Mater.* **2023**, *22*, 1507−1514.

(12) Chen, H.; Liu, C.; Xu, J.; Maxwell, A.; Zhou, W.; Yang, Y.; Zhou, Q.; Bati, A. S. R.; Wan, H.; Wang, Z.; Zeng, L.; Wang, J.; Serles, P.; Liu, Y.; Teale, S.; Liu, Y.; Saidaminov, M. I.; Li, M.; Rolston, N.; Hoogland, S.; Filleter, T.; Kanatzidis, M. G.; Chen, B.; Ning, Z.; Sargent, E. H. Improved charge extraction in inverted perovskite solar cells with dual-site-binding ligands. *Science* **2024**, *384* (6692), 189−193.

(13) Akman, E.; Shalan, A. E.; Sadegh, F.; Akin, S. Moisture-Resistant $FAPbI_3$ Perovskite Solar Cell with 22.25% Power Conversion Efficiency through Pentafluorobenzyl Phosphonic Acid Passivation. *ChemSusChem* **2021**, *14* (4), 1176−1183.

(14) Krishna, A.; Škorjanc, V.; Dankl, M.; Hieulle, J.; Phirke, H.; Singh, A.; Alharbi, E. A.; Zhang, H.; Eickemeyer, F.; Zakeeruddin, S. M.; Manjunatha Reddy, G. N.; Redinger, A.; Rothlisberger, U.; Grätzel, M.; Hagfeldt, A. Mitigating the Heterointerface Driven Instability in Perovskite Photovoltaics. *ACS Energy Lett.* **2023**, *8* (8), 3604−3613.

(15) Han, G.; Ming Koh, T.; Li, J.; Febriansyah, B.; Fang, Y.; Jamaludin, N. F.; Fong Ng, Y.; Singh Rana, P. J.; Mhaisalkar, S.; Mathews, N. Toward Efficient and Stable Perovskite Photovoltaics with Fluorinated Phosphonate Salt Surface Passivation. *ACS Appl. Energy Mater.* **2021**, *4* (3), 2716−2723.

(16) Li, F.; Deng, X.; Qi, F.; Li, Z.; Liu, D.; Shen, D.; Qin, M.; Wu, S.; Lin, F.; Jang, S. H.; Zhang, J.; Lu, X.; Lei, D.; Lee, C. S.; Zhu, Z.; Jen, A. K. Y. Regulating Surface Termination for Efficient Inverted Perovskite Solar Cells with Greater Than 23% Efficiency. *J. Am. Chem. Soc.* **2020**, *142* (47), 20134−20142.

(17) Dunbar, R. B.; Duck, B. C.; Moriarty, T.; Anderson, K. F.; Duffy, N. W.; Fell, C. J.; Kim, J.; Ho-Baillie, A.; Vak, D.; Duong, T.; Wu, Y.; Weber, K.; Pascoe, A.; Cheng, Y.; Lin, Q.; Burn, P. L.; Bhattacharjee, R.; Wang, H.; Wilson, G. J. How reliable are efficiency measurements of perovskite solar cells? The first inter-comparison, between two accredited and eight non-accredited laboratories. *J. Mater. Chem. A* **2017**, *5* (43), 22542−22558.

(18) Senevirathna, D. C.; Yu, J. C.; Nirmal Peiris, T. A.; Li, B.; Michalska, M.; Li, H.; Jasieniak, J. J. Impact of Anion Impurities in Commercial PbI_2 on Lead Halide Perovskite Films and Solar Cells. *ACS Materials Lett.* **2021**, *3* (4), 351−355.

(19) Park, K.; Tan, S.; Kodalle, T.; Lee, D. K.; Abdelsamie, M.; Park, J. S.; Lee, J. H.; Jung, S. K.; Ko, J. H.; Park, N. G.; Sutter-Fella, C. M.; Yang, Y.; Lee, J. W. Atmospheric Humidity Underlies Irreproducibility of Formamidinium Lead Iodide Perovskites. *Adv. Mater.* **2024**, *36* (14), No. 2307265.

(20) Baumann, D. O.; Laufer, F.; Roger, J.; Singh, R.; Gholipoor, M.; Paetzold, U. W. Repeatable Perovskite Solar Cells through Fully Automated Spin-Coating and Quenching. *ACS Appl. Mater. Interfaces* **2024**, *16* (40), 54007−54016.

(21) Hong, M. J.; Labram, J. G. Inter-Sample and Intra-Sample Variability in Electronic Properties of Methylammonium Lead Iodide. *Adv. Funct. Mater.* **2021**, *31* (21), No. 2101843.

(22) Taylor, A. D.; Sun, Q.; Goetz, K. P.; An, Q.; Schramm, T.; Hofstetter, Y.; Litterst, M.; Paulus, F.; Vaynzof, Y. A general approach to high-efficiency perovskite solar cells by any antisolvent. *Nat. Commun.* **2021**, *12*, 1878.

(23) Tang, L.; Wang, X.; Liu, X.; Zhang, J.; Wang, S.; Zhao, Y.; Gong, J.; Li, J.; Xiao, X. Mixed Solvents Assisted Post-Treatment Enables High-Efficiency Single-Junction Perovskite and 4T Perovskite/CIGS Tandem Solar Cells. *Advance Science* **2022**, *9* (23), No. 2201768.

(24) Worsley, C.; Potts, S.-J.; Hughes, D.; Tsoi, W. C.; Watson, T. Age-induced excellence with green solvents: the impact of residual solvent and post-treatments in screen-printed carbon perovskite solar cells and modules. *Mater. Adv.* **2024**, *5* (10), 4354−4365.

(25) Zheng, R.; Li, J.; Li, S.; He, B.; Chen, S. Dipole orientation-induced interfacial energy level alignment difference in 2D perovskite passivated 3D perovskite by in situ investigation. *Sustain. Energy Fuel.* **2025**, *9* (14), 3831−3837.

(26) Haque, M. D.; Troughton, J.; Baran, D. Processing-Performance Evolution of Perovskite Solar Cells: From Large Grain Polycrystalline Films to Single Crystals. *Adv. Energy Mater.* **2020**, *10* (13), No. 1902762.

(27) Li, C.; Zhang, N.; Gao, P. Lessons learned: how to report XPS data incorrectly about lead-halide perovskites. *Mater. Chem. Front.* **2023**, *7* (18), 3797−3802.

(28) Liang, J.; Hu, X.; Wang, C.; Liang, C.; Chen, C.; Xiao, M.; Li, J.; Tao, C.; Xing, G.; Yu, R.; Ke, W.; Fang, G. Origins and influences of metallic lead in perovskite solar cells. *Joule* **2022**, *6* (4), 816−833.

(29) Zhao, X.; Qiu, Y.; Wang, M.; Wu, D.; Yue, X.; Yan, H.; Fan, B.; Du, S.; Yang, Y.; Yang, Y.; Li, D.; Cui, P.; Huang, H.; Li, Y.; Park, N. G.; Li, M. Regulation of Buried Interface through the Rapid Removal of PbI_2·DMSO Complex for Enhancing Light Stability of Perovskite Solar Cells. *ACS Energy Lett.* **2024**, *9* (6), 2659−2669.

https://doi.org/10.1021/acsaem.5c03857
ACS Appl. Energy Mater. 2026, 9, 2701−2708